Delft University of Technology

Effects of root Gurney flaps on the aerodynamic performance of a horizontal axis wind turbine

Zhang, Ye; Ramdoss, Varun; Saleem, Zohaib; Wang, Xiaofang; Schepers, Gerard; Ferreira, Carlos

Important note
To cite this publication, please use the final published version (if applicable).
Please check the document version above.

Effects of root Gurney flaps on the aerodynamic performance of a horizontal axis wind turbine

Ye Zhang [a, b, *], Varun Ramdoss [a], Zohaib Saleem [a], Xiaofang Wang [b], Gerard Schepers [c], Carlos Ferreira [a]

[a] DUWIND, Faculty of Aerospace Engineering, Delft University of Technology, Kluyverweg 1, 2629HS, Delft, the Netherlands
[b] School of Energy and Power Engineering, Dalian University of Technology, Dalian, 116024, China
[c] ECN, Westerduinweg 3, 1755 LE Petten, the Netherlands

A B S T R A C T

This paper presents a computational investigation on the effects of Gurney flaps on the aerodynamic performance of a horizontal axis wind turbine, which is part of the EU FP7 AVATAR project. The research investigates two configurations of Gurney flaps applied at the inboard part of the blade ($r/R = 0.30 \sim 0.46$) at 85% chord location on the pressure surface. The computational method applied in the investigation solves the Reynold-Averaged Navier-Stokes (RANS) equations with multiple reference frame (MRF) approach, which models the rotating turbulent flow over the wind turbine rotor. Numerical simulations are performed for the wind turbine rotor with and without Gurney flap at the tip speed ratios $\lambda = 4.59$ and 6.35. Comparison of the numerical results with experimental measurements shows that the deployment of Gurney flaps effectively increases the power coefficients of the rotor by 21% at $\lambda = 6.35$. Gurney flaps have a considerable 3D effect on spanwise thrust and torque coefficients distribution. The performance of two Gurney flaps configurations is compared. It is shown that the larger Gurney flap reduces the effect on the power generated due to protruding out of the local boundary layer of the flow. The numerical results are in good agreement with the experimental results in terms of total thrust and power within 14.1% difference, and complement the experimental database.

© 2019 Elsevier Ltd. All rights reserved.

1. Introduction

Over the past few decades, the use of wind energy as a mainstream source of energy has increased. Total capacity of wind power installed in 2015 in the European Union (EU) was 315 Twh approximately, which could potentially cover 11.4% of the total electricity consumption of the EU in a normal wind year [1]. In order to further decrease the cost of energy (COE), the size of wind turbine rotor becomes significantly larger and will be upscaled towards 10−20 *MW* to capture more energy from wind. Meanwhile, scientific researchers and professional engineers are making great efforts to apply advanced flow control techniques to improve the aerodynamic performance of large wind turbine rotors [2]. To achieve this, the AVATAR (AdVanced Aerodynamic Tools of lArge Rotors) project was initiated by EERA (European Energy Research

Alliance), started in November 2013 and ended in December 2017 [3]. The overall objective of the AVATAR project was to evaluate, validate and improve aerodynamic and aero-elastic tools to ensure applicability for large wind turbines [4,5]. The capabilities of the resulting tools were demonstrated on a large scale rotor with and without flow control devices [6]. These devices include active and passive flow type devices, which act on the wind turbine blade to achieve lift increase and/or drag reduction. The intention of using flow control devices lies in the requirement for improving the wind turbine rotor performance.

Gurney flaps are one category of passive flow devices used to effectively improve the design lift coefficients of isolated airfoils, particularly at high lift coefficients. The early days of studying flow physics of Gurney flap test cases was primarily carried out by using experimental techniques. Initial flow measurements on Gurney flaps were carried out by Liebeck in his seminal work on high lift systems [7]. The flow structure in the presence of a Gurney flap on an airfoil was illustrated by Liebeck (Fig. 1). The formation of a separated region in front of the Gurney flap is followed by the

Nomenclature

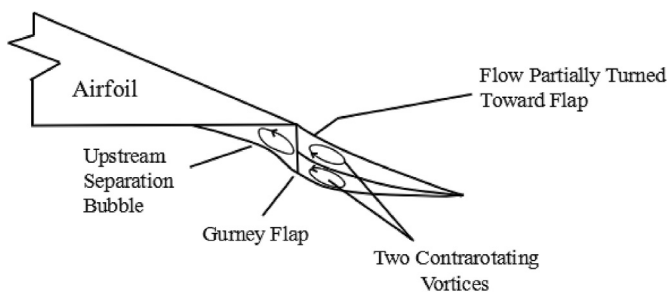|	
Γ	Circulation [m$^2/s$]
λ	Tip speed ratio [$-$]
θ	Pitch angle [$°$]
B	Number of blade [$-$]
C_P	Power coefficient -]
C_p	Pressure coefficient [$-$]
C_Q	Torque coefficient [$-$]
C_T	Thrust coefficient [$-$]
n	Rotational speed [rpm]
R	Rotor radius [m]
r	Local radius [m]
Re	Reynolds number [$-$]
Tu	Turbulence intensity [%]
U_∞	Free-steam velocity [m/s]

Fig. 1. Flow structure around a Gurney flap, adapted from Ref. [7].

formation of two counter rotating vortices behind the Gurney flap which helps in wake compression and off-the-surface pressure recovery [7]. The Kutta condition [8] for an airfoil mentions that for an airfoil with a finite trailing edge angle, then the trailing edge acts as the rear stagnation point for the flow [8]. In the case of Gurney flaps, the Kutta condition is shifted to a point off the surface of the airfoil [9,10], thereby allowing for the flow on the top surface of the airfoil to resist the adverse pressure gradient and increase the lift by postponing separation and stall of the airfoil/wing system. Cory et al. [11] further suggested that the low pressure region behind the Gurney flap causes a downward momentum of fluid in the region above the trailing edge. They also concluded that the small separation region on the suction side of the airfoil has the benefit of counteracting the drag caused by the Gurney flap. In past years, the performance of isolated airfoils with Gurney flaps have been investigated at high subsonic Mach numbers and high Reynolds numbers, low Reynolds number, low Mach number by many researchers [12]. The addition of a Gurney flap was shown to improve airfoil performance at high lift coefficients in particular. The drag coefficient of the airfoil was found to increase at low lift coefficients only. Kentfield [13] conducted a detailed experimental study of the flow field over the downstream portion of an NACA 0015 airfoil over a range of incidence angles up to $10°$. The apparent wake vortex shedding frequency of the airfoil equipped with $1.5\%c$ length Gurney flap was about 35% of that generated by the rounded truncated trailing edge of equal thickness. In terms of numerical investigations on Gurney flaps, Jain et al. [14] utilized the one-equation Baldwin-Barth turbulence model for the computational analysis of the Gurney flap on the NACA 4412 airfoil. They deducted an increase in lift coefficient and nose down pitching moment with

the presence of Gurney flaps. They also stated that the increase in Gurney flap height brought about an increase in lift at the expense of increasing drag. The research suggested that the flap heights less than 1.25% chord lead to increase in lift with very little increase in drag along with the suggestion that the separation point of the flow moves aft with the attachment of Gurney flap. Gigure et al. [15] stated that efficient Gurney flaps are always found to have a height not greater than the boundary layer thickness. Patel [16] studied the computational analysis of NACA 0012 airfoils with Gurney flaps by using S-A and $k - \omega$ SST turbulence models. The research suggested that the S-A model was appropriate for low Reynolds number and high angles of attack simulations, followed by the $k - \omega$ SST model which provides a better suit for analysis.

Although studies show that the root section of the horizontal axis wind turbine (HAWT) blades contribute to a less amount of the total power generated when compared with the tip section of the blade, the aerodynamic loss at the inboard part of the blade is more than half of total blade aerodynamic loss. This is due to large separated flow and transitional geometry which might not be an effectively aerodynamic design airfoil due to structural requirements. The root section forms a transition from a thick airfoil to a circular blade, which is connected to the root hub. Flow separation and dynamic stall phenomenon normally occur in this particular region, even in the condition that wind turbine is operating at an optimal tip speed ratio. The detailed particle image velocimetry (PIV) experiment of a wind turbine root flow conducted by Akay [17] clearly showed the highly three-dimensional flow field at the inboard part of the blade, and strong radial flow was observed in this region. Comprehensive root flow visualizations of CFD simulations from many researchers [18–21] also indicated that highly separated flow exits near the blade root. On one hand, such unsteady separated flow decreases the lift and therefore reduces the aerodynamic performance of the wind turbine rotor. On the other hand, the fluctuating aerodynamic loads caused by the highly unsteady flow can significantly affect the lifetime of the wind turbine blade. Therefore, it is vital to apply flow control techniques, such as Gurney flaps, to reduce the separated flow in the root region, to decrease the root loss and eventually to improve the aerodynamic performance of the wind turbine rotor. Kentfield [22] predicted the performance of a wind turbine model equipped with full span Gurney flaps at a low blade-chord-based Reynolds number of 6×10^4. Very significant performance improvement was observed by using Gurney flaps. Another test of a Nordtank 65 kW full-scale wind turbine equipped with Gurney flaps increased the monthly output by 4.3%. Recently, Ebrahimi [23] numerically investigated the NREL Phase VI, a stall-regulated upwind wind turbine equipped with microtab as a passive flow control device. Greater impact on the rotor performance was observed when locating microtabs at the outboard part of the blade than the inboard part. 17% of wind energy was saved by using a mictab with appropriate spanwise height distribution. A critical study on passive flow control techniques for straight-bladed vertical axis wind turbine was given by Zhu et al. [24]. A Gurney flap with inward dimple on the lower surface near the trailing edge airfoil increased the average tangential force by 35% in steady case and 40% in oscillating case [25]. Regarding the effects of Gurney flaps on vertical axis wind turbine performance, higher thrust and more efficient extraction of wind energy were observed by adding Gurney flap.

To summarize the research gap, the existing research of Gurney flaps is mainly applied on 2D (wind turbine) airfoils. The usage of Gurney flaps is very limited for full 3D wind turbine rotor, especially at the root region. Therefore, this research will mainly focus on investigating the aerodynamic characteristics of a HAWT system with Gurney flaps placed near the root section of the blade. The aim

is to answer the following questions:

- How do root Gurney flaps influence the distribution of critical aerodynamic characteristics on varying cross-sections of a rotating HAWT blade?
- How do the spanwise aerodynamic loading and the performance of a HAWT blade vary with root Gurney flaps height?
- What is the capability of an open source CFD tool to predict the aerodynamic performance of a horizontal axis wind turbine configured with root Gurney flaps?

2. Methodology

2.1. Wind turbine rotor model

A cropped, modified and scaled version of the LM38.8 rotor blade of the Neg Micon NM80 wind turbine system is investigated in this work. The studied blade is $0.85m$ in height with a twist and chord distribution as shown in Fig. 2. Three different airfoil profiles exist along the span of the blade. From the root to the tip, they are the DU99-W-405LM airfoil from 35% to 50% span, the NACA-63424 airfoil from 55.5% to 75.5% span and the NACA-63421 airfoil from 82.5% span to the tip. The schematic drawing of the blade can be further understood from Fig. 3 where the varying sections of the blade have been identified.

2.2. Gurney flap configurations

Two Gurney flap configurations, referring to *sp*1 and *sp*2, are investigated to identify their effect on the aerodynamic performance of the horizontal axis wind turbine. The specifications of Gurney flaps are listed in Table 1 and the detailed dimensions of the *sp*1 and *sp*2 geometries are illustrated in Fig. 4. The flaps are applied at 85% chord location and at a height of $0.3m$ from the axis of rotation to a height $0.46m$ ($r/R = 0.30 \sim 0.46$).

2.3. Numerical set-up

The more detailed information of the investigated rotor and simulated conditions are shown in Table 2. The computational domain considered for the numerical simulations involves a cylindrical domain around the wind turbine blade and two semi-cylindrical domains of increasing sizes. A structured type of

boundary layer mesh is created around the wind turbine blade domain, whereas an unstructured meshing topology is utilized for the two remaining semi-cylindrical domains. More than 20 computational nodes are applied in the structured boundary layer grid to capture viscous flow near the blade. The schematic layout of the computational domain and mesh topology is shown in Fig. 5 and the tip mesh topology of the Gurney flap is present in Fig. 6.

An incompressible, steady-state RANS equations within Open-FOAM are solved to model fully turbulent flow over the wind turbine. The system of RANS equations is closed with two equations turbulence model $k - \omega$ SST [26], which is suitable for predicting adverse pressure gradient flows and moderate separated flows. The RANS equations are decoupled and solved with the SIMPLE (Semi-Implicit Method for Pressure-Linked Equations) algorithm, proposed by Patankar et al. [27]. The Multiple reference frame (MRF) approach is applied to model the rotating flow by adding the Coriolis force in the momentum equations for the MRF zones. The advective terms of velocity and turbulent quantities are discretized by using the second order upwind scheme *linearUpwind* [28]. The discretization of the diffusion terms in the momentum equations is carried out by using *linear limited* 0.33 [28].

A Dirichlet boundary condition is set at the inlet for the inflow velocity and turbulent inflow variables, and a zero gradient Neumann boundary condition is set for the pressure. Zero gradient boundary condition is imposed at the outlet for all variables, except for the pressure for which a Dirichlet condition with a zero mean is used [29]. Euler inviscid wall conditions are used at the hub surfaces in order to reduce the total grid size, while no-slip wall boundary conditions are applied at the surfaces of rotor blades. Arbitrary mesh interface (AMI) technology [30] is imposed at the interfaces connecting the MRF rotating zone and stationary zone. A zero gradient is used for the fareld boundary of the computational domain.

3. Results and discussion

A verification and validation study is firstly introduced to evaluate the prediction capability of CFD model for wind turbine simulation with Gurney flaps.

3.1. Grid independence study

The grid independence study is performed for the configurations of the wind turbine with a clean blade and Gurney flap blades.
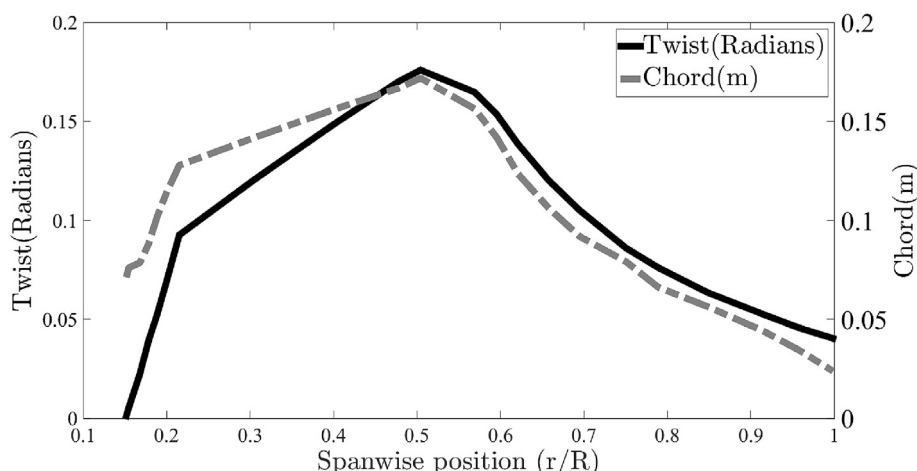

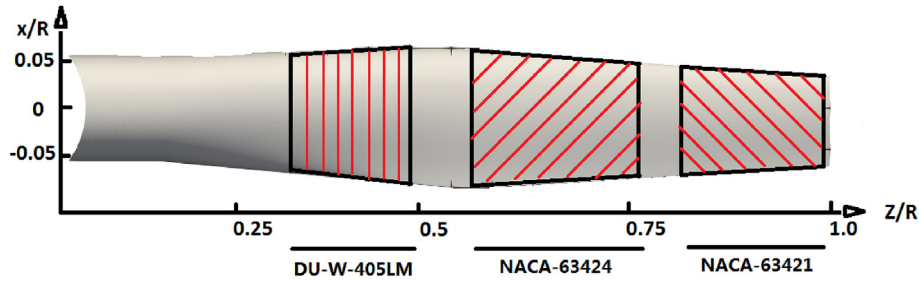**Fig. 2.** Twist and chord distributions of the wind turbine rotor model.

Fig. 3. Cropped, modified and scaled version of the LM38.8 blade sections.

Table 1
Specifications of Gurney flaps.

	h_1	l_1	l_2	h_2	θ
$sp1[mm]$	10	10	1.5	1.5	55°
$sp2[mm]$	20	10	1.5	1.5	55°
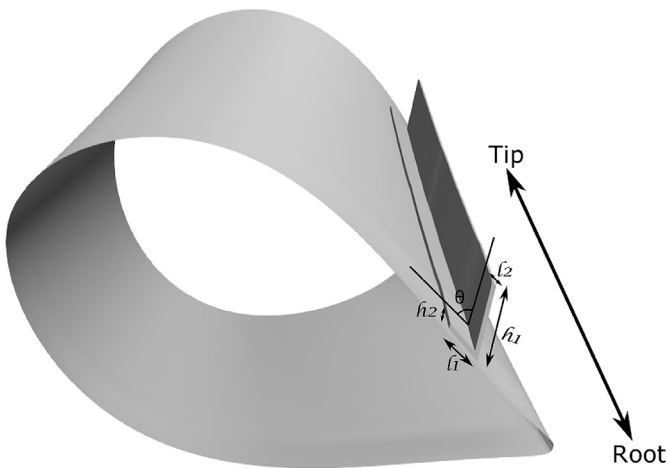
Fig. 4. Schematic drawing of the Gurney flaps.

Table 2
Blade geometry and simulated conditions.

Number of blade $B[-]$	2
Rotor radius $R[m]$	1.0
Hub radius $r_{hub}[m]$	0.15
Twist angle at $r/R = 0.40[°]$	8.6
Turbulence intensity $Tu[\%]$	0.05
Rotational speed $n[rpm]$	350, 485
Free-steam velocity $U_\infty[m/s]$	8
Tip speed ratio $\lambda[-]$	4.59, 6.35
Tip Reynolds number $Re_{tip}[-]$	$(2.5 \sim 3.5) \times 10^6$
Pitch angle $\theta[°]$	0

A numerical simulation of the wind turbine with clean blades operating at the tip speed ratio of $\lambda = 4.59$ is performed to investigate the grid sensitivity. Table 3 lists the detailed grid characteristics in the simulation. Three different levels of grids are generated to carry out the grid independence study. The thrust coefficient C_T is used to identify that the solutions achieve spatial convergence. As seen from Table 4, a good agreement of calculated C_T is obtained between a medium mesh and a fine mesh. Therefore, the fine mesh is considered sufficient for the mesh independence study. The computational results of wind turbine simulation with a clean blade shown in Table 5 below are the numerical solutions obtained

on this fine mesh.

Similarly, the same procedures are performed on the numerical simulations of the wind turbine with Gurney flaps to check the grid independence. The mesh sensitivity study has been conducted only for the $sp1$ gurney flap at 85% chord location. The fine mesh with the converged solution has total cells of 13.5×10^6, 480 nodes in the chordwise direction and 250 nodes in the spanwise direction. The calculated power coefficient C_T of the wind turbine with the Gurney flap $sp1$ is 0.5432. The remaining Gurney flap configuration $sp2$ has been adopted with the fine mesh strategy which is used for the $sp1$ configuration at 85% chord location with the only difference being the node distribution on the $sp2$ Gurney flap (~ 2 times $sp1$ Gurney flap).

3.2. Verification and validation study

The verification study is performed by a code-to-code comparison. A blade element moment theory (BEMT) with a Prandtl tip loss model calculation was carried out to verify the loads on sections over the blade close to the mid-span region which has flow similar to that of a clean case blade in the CFD simulation. The sections of the $sp1$ case HAWT blade at heights of $0.70m$, $0.75m$ and $0.80m$ have been selected for the BEMT comparison study at a tip speed ratio of 6.35. Table 5 shows the numerical results of BEMT calculation and CFD simulation. Good agreements can be seen between the BEMT results and CFD simulations for all three sections with a maximum relative difference of 6.67%. The difference presents an expected increase with a larger aspect ratio of the blade in which more tip correction is required. The increase in difference is contributed to the result of ensuing tip vortices from the blade tip and BEMT methodology normally suffers from modeling three-dimensional blade tip flow accurately.

Following the verification study, a comprehensive comparison between the CFD numerical result and experimental measurement is carried out. The measurement of wind turbine aerodynamic performance at two different tip speed ratios (TSR) is performed in the Open Jet Facility (OJF) of Delft University of Technology, both for the clean blade and Gurney flap cases. Tables 6–8 list the computational results, measured data and their relative difference (ε) for the clean case and Gurney flaps ($sp1$ & $sp2$) configurations, respectively. A fair good agreement can be seen for most cases within 10% the relative difference, except for the $sp2$ Gurney flap configuration with $\lambda = 6.35$, which has a larger relative difference of 14.136%. The main reason could be that CFD simulation does not model the effect of ZigZag tape which affects the aerodynamic loads on blades in the experiment and therefore CFD results in a higher power coefficient. Fig. 7 compares the thrust and power coefficients of numerical result and experimental measurement for the wind turbine. In the $C_T - \lambda$ plot, CFD prediction shows the same trend as the wind tunnel measurement, obtaining a higher value of C_T and lower C_P at larger TSR. Thrust coefficient C_T is increased by deployment of
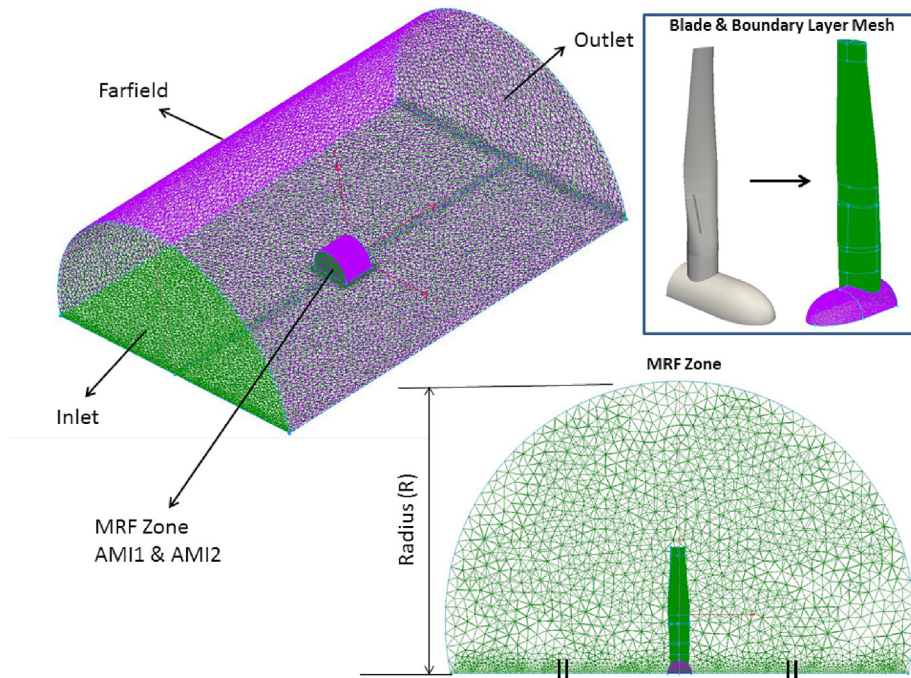
Fig. 5. Schematic of the computational domain and mesh topology.

Gurney flaps for each TSR, and the larger $sp2$ Gurney flap configuration has a higher C_T compared to the $sp1$ Gurney flap case both for $\lambda = 4.59$ and $\lambda = 6.35$. In terms of the Gurney flap effect on C_P, the power coefficient of the wind turbine increases to some extent by adding Gurney flap devices. The $sp2$ configuration has almost the same effect on power increment as the $sp1$ at the design TSR $\lambda = 4.59$, but plays a less important role in increasing the power at the higher TSR $\lambda = 6.35$. The reason for the reduction in power with the
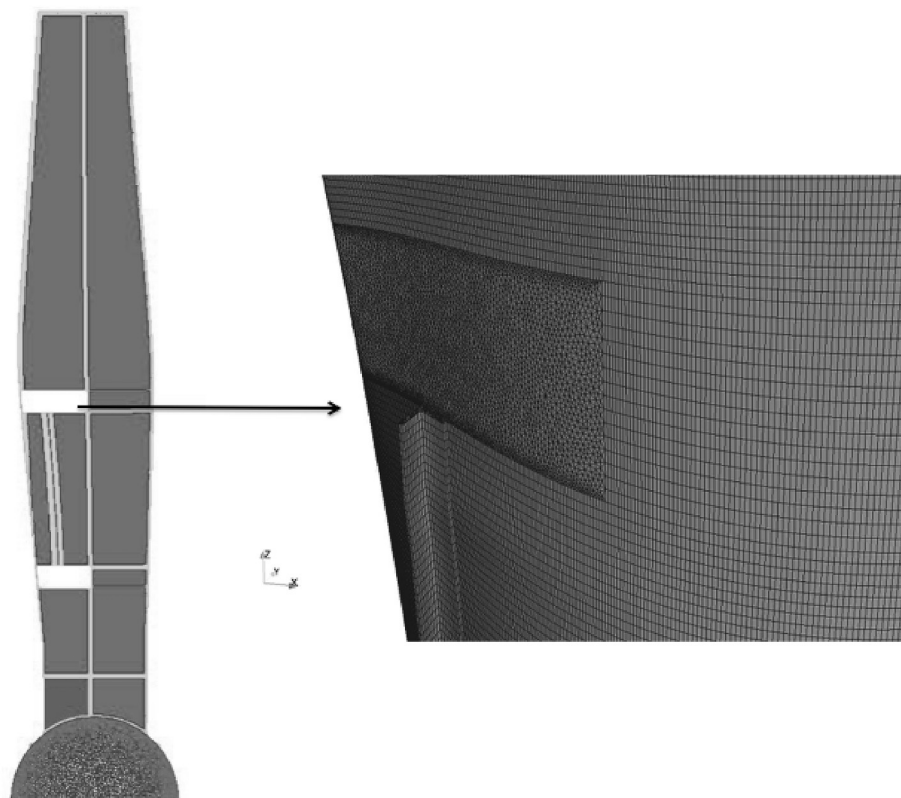
Fig. 6. Gurney flap tip mesh topology.

Table 3
The characteristics of three different levels of computational grids.

grid characteristics	coarse	medium	fine
chordwise nodes	200	300	400
spanwise nodes	100	150	200
y^+	$4 \sim 5$	$4 \sim 5$	$4 \sim 5$
total cells	5.6×10^6	7.2×10^6	8.5×10^6

Table 4
Thrust coefficient of C_T for the wind turbine with clean blade at $\lambda = 4.59$ on three different levels of computational grids.

	Coarse	medium	fine
C_T	0.4436	0.4825	0.4938

Table 5
Comparison CFD and BEMT at $\lambda = 6.35$

r/R	aspect ratio (r/c)	$C_{T(BEMT)}$	$C_{T(CFD)}$	difference(%)
0.70	5.5	0.329	0.34199	3.9483
0.75	7.0	0.354	0.3719	5.0564
0.80	9.0	0.395	0.4221	6.6734

Table 6
Comparison of thrust and power coefficients between CFD and experiment for the clean configuration at $\lambda = 4.59$

	CFD	Experiment	$\varepsilon[\%]$
C_T	0.4938	0.5138	-3.8987
C_P	0.2473	0.2425	1.9793

Table 7
Comparison of thrust and power coefficients between CFD and experiment for the clean configuration at $\lambda = 6.35$

	CFD	Experiment	$\varepsilon[\%]$
C_T	0.6352	0.5956	6.6488
C_P	0.1760	0.1613	9.1130

Fig. 7. C_T and C_P for the clean and Gurney flap cases.

An increase in the suction peak and the positive pressure at the local presence of the Gurney flap is observed. The $sp2$ Gurney flap has a higher suction peak at $\lambda = 4.59$ whereas the $sp1$ Gurney flap has a higher suction peak at $\lambda = 6.35$ on the spanwise location $r/R = 0.35$ and 0.4. A slightly higher suction peak is still observed at $r/R = 0.6$ even if there is no Gurney flap deployment. As the radial location increases to $r/R = 0.8$, the Gurney flaps which locate near the root region have a tiny effect on cross-section pressure distribution.

Table 8
Comparison of thrust and power coefficients between experiment and CFD for the Gurney flap configurations.

		$\lambda = 4.59$			$\lambda = 6.35$		
		Experiment	CFD	$\varepsilon[\%]$	Experiment	CFD	$\varepsilon[\%]$
$sp1$	C_T	0.5809	0.5432	-6.4899	0.2600	0.2694	3.6153
	C_P	0.7044	0.6564	-6.8143	0.199	0.2096	5.3266
$sp2$	C_T	0.6198	0.5608	-9.5191	0.2668	0.2830	6.0441
	C_P	0.7400	0.7168	-3.1418	0.1818	0.2075	14.136

increase in Gurney flap height (exception at TSR_{design}) would be due to the larger Gurney flap ($sp2$) protruding out of the local boundary layer of the flow thereby reducing its effect on the power generated.

3.3. Pressure coefficient distribution

The cross-section pressure distributions along the span of blade are identified for the clean and Gurney flap cases. The C_p distributions at $r/R = 0.35, 0.4, 0.6$ and 0.8 are illustrated in Figs. 8–11.

Gurney flaps greatly increase the pressure difference between the suction side and the pressure side in the vicinity of spanwise deployment locations. This influence can be seen in the C_p comparison at the spanwise locations of $r/R = 0.35$ and 0.40 in Fig. 8.
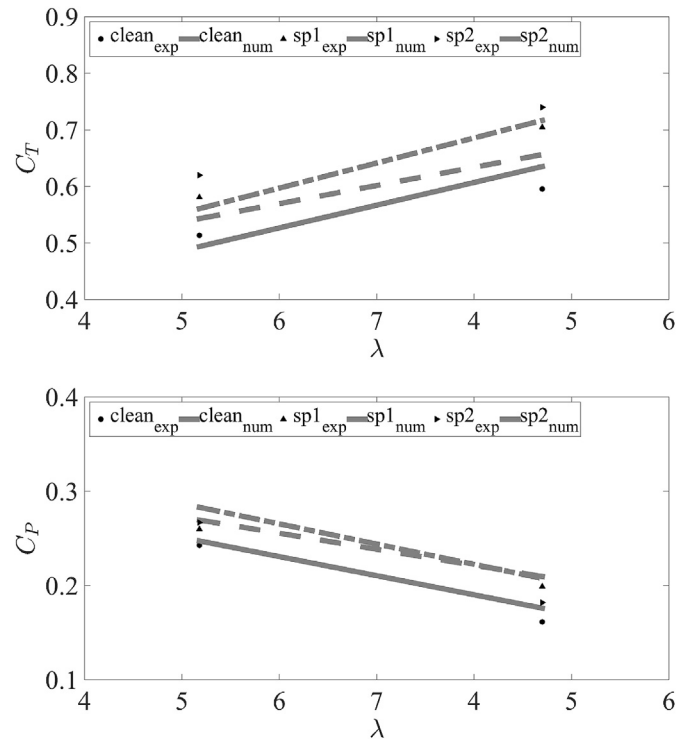
3.4. Separation location study

Fig. 12 shows the distribution of flow separation location on the suction side of the airfoil over the entire span of the blade. The Gurney flap region is indicated by the highlighted box in these plots. The separation locations are identified by the location where the coefficient of friction is zero or close to zero. As expected, Gurney flaps delay the flow separation on the suction side and move the separation locations aft. The larger Gurney flap $sp2$ increases the effect on shifting the separation location towards the trailing edge as compared to the smaller Gurney flap $sp1$. Moreover, the difference in shift of the separation location between the two Gurney flaps tends to increase with the increase in tip speed ratio of
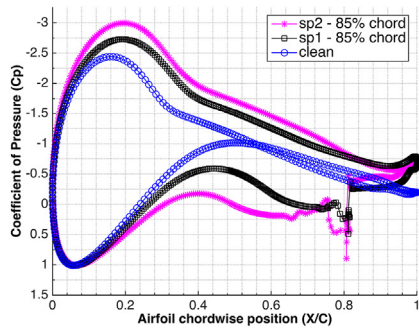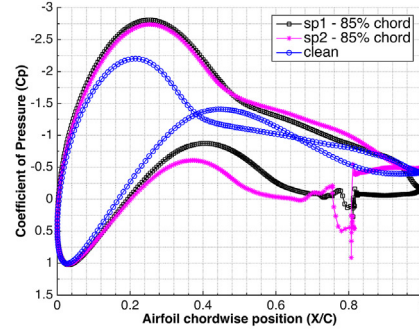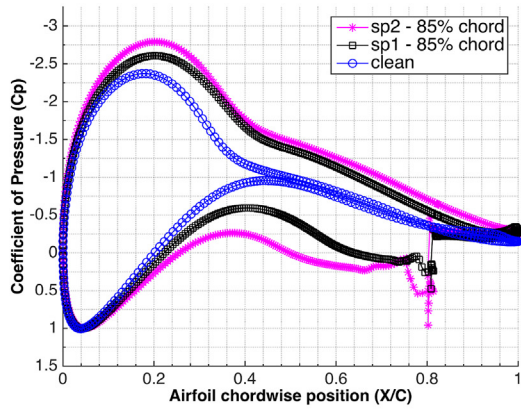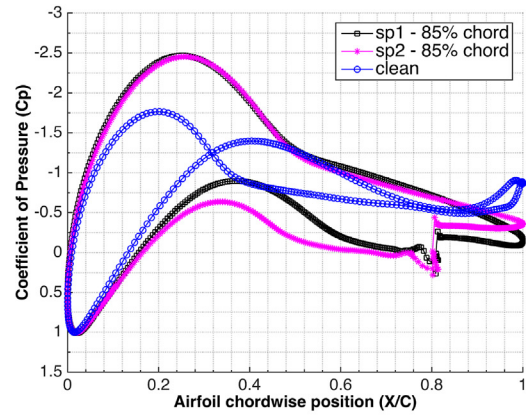
(a) $\lambda = 4.59$ (b) $\lambda = 6.35$

Fig. 8. C_p distribution at $r/R = 0.35$ with $\lambda = 4.59$ and $\lambda = 6.35$

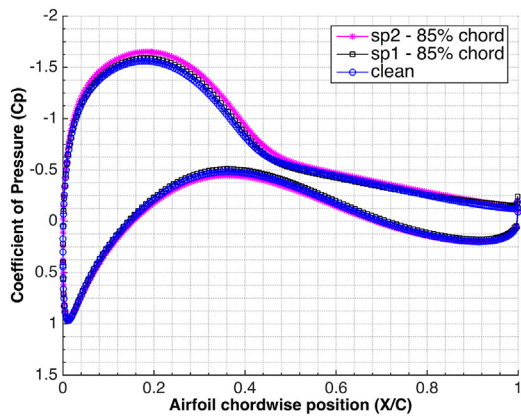(a) $\lambda = 4.59$ (b) $\lambda = 6.35$
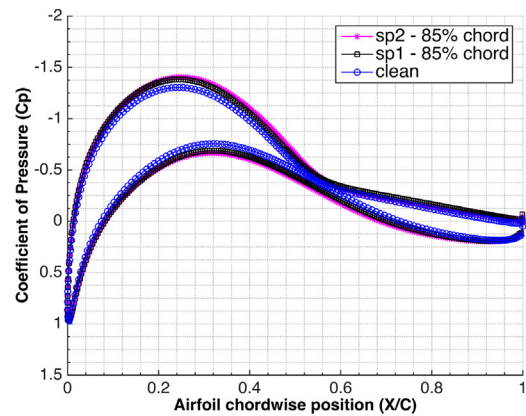
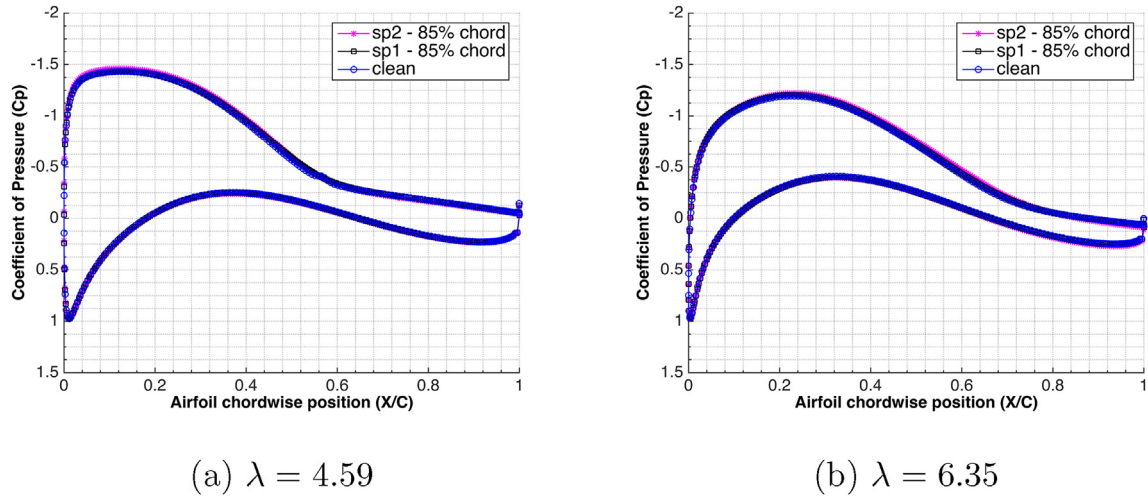**Fig. 9.** C_p distribution at $r/R = 0.40$ with $\lambda = 4.59$ and $\lambda = 6.35$

(a) $\lambda = 4.59$ (b) $\lambda = 6.35$

Fig. 10. C_p distribution at $r/R = 0.60$ with $\lambda = 4.59$ and $\lambda = 6.35$

(a) $\lambda = 4.59$ (b) $\lambda = 6.35$

Fig. 11. C_p distribution at $r/R = 0.80$ with $\lambda = 4.59$ and $\lambda = 6.35$

the wind turbine.

3.5. Three dimensional flow

Figs. 13 and 14 show the relative velocity flow fields at $r/R = 0.4$ with two different tip speed ratios in the rotating reference frame. The recirculation regions created as a result of separation over the suction side of the sectional airfoil can be clearly seen in the baseline rotor without Gurney flap configuration. By deploying Gurney flaps, the downward shift of the Kutta condition (off-the-surface pressure recovery) is substantiated in these flow field visualization plots. As a result, the separation location over the airfoil also tends to shift towards the trailing edge of the airfoil for the Gurney flap configurations. The shift of the separation location tends to increase with Gurney flap height as well as tip speed ratio.

3.6. Thrust and torque coefficient

The thrust and torque coefficients have been calculated by using:

$$C_T = \frac{AxialForce}{0.5 \times \rho \times U_\infty^2 \times 2\pi r} \tag{1}$$

$$C_Q = \frac{TangentialForce}{0.5 \times \rho \times U_\infty^2 \times 2\pi r^2} \tag{2}$$

Figs. 15 and 16 show the coefficients of thrust and torque for the wind turbine blade over the span of the blade predicted by CFD simulations. The plots show the increase in thrust coefficient at the local region of the Gurney flap. The $sp2$ configuration has a higher thrust coefficient value as compared to the $sp1$ configuration. The difference in thrust between the two configurations becomes larger with the increase in TSR values. The $sp2$ Gurney flap configuration seems to provide a higher thrust as compared to the $sp1$ Gurney flap configuration. The reason could be attributed to the increase in airfoil section wetted area for the $sp2$ configuration in regards to the sp1 configuration which might lead to an increase in pressure and viscous forces along the streamwise direction.

The C_Q plots show the increase in torque at the region of the Gurney flaps. The sp2 configuration provides a higher torque at the Gurney flap location as compared to the $sp1$ configuration at $\lambda =$
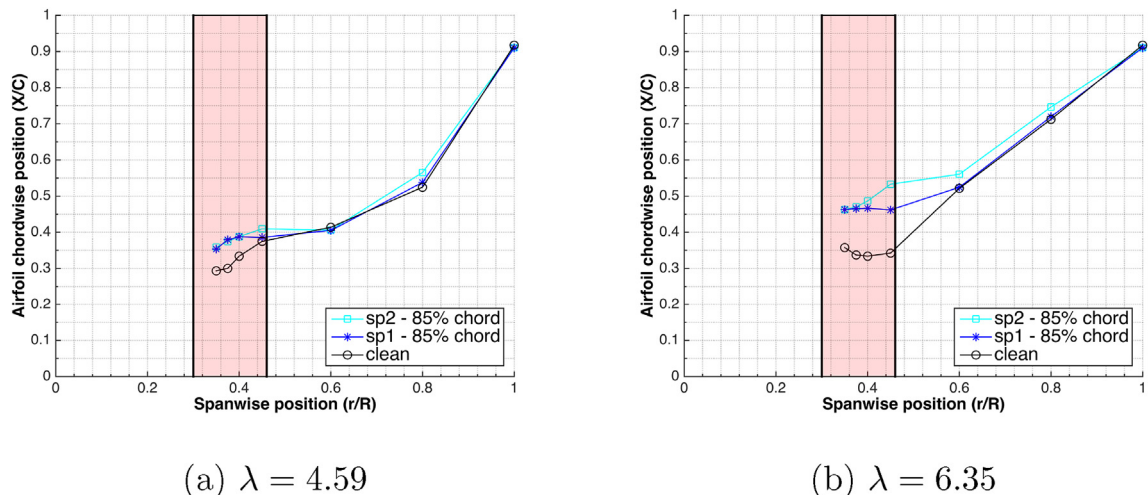

(a) $\lambda = 4.59$ (b) $\lambda = 6.35$

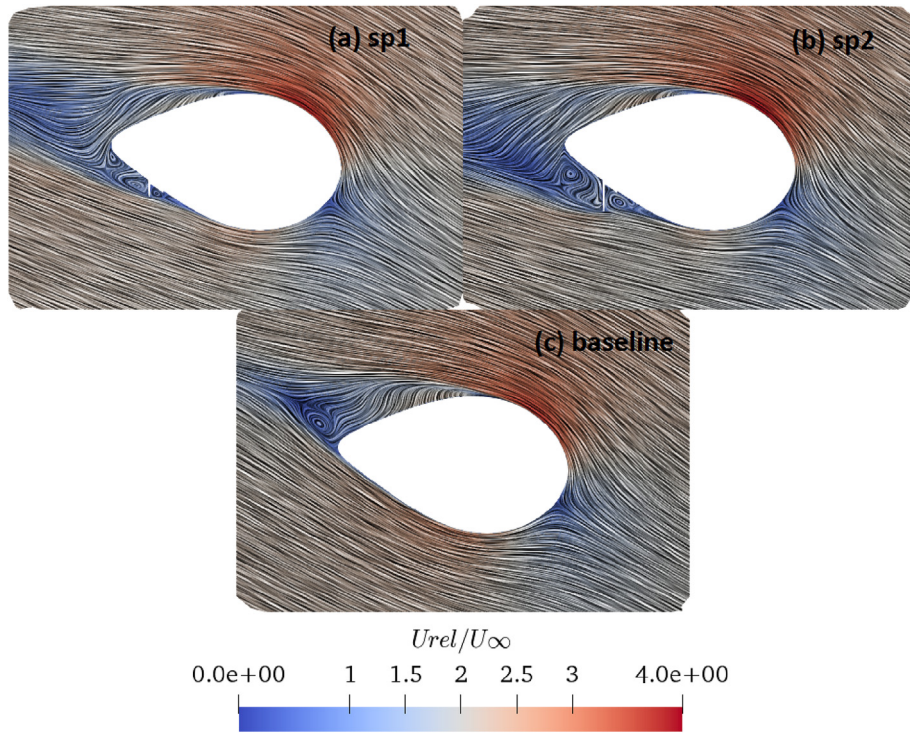**Fig. 12.** Separation location distribution at $\lambda = 4.59$ and 6.35.

Fig. 13. Relative velocity flow field at $r/R = 0.4$ with $\lambda = 4.59$, (a) $sp1$ Gurney flap, (b) $sp2$ Gurney flap, (c) baseline rotor.

4.59. The trend seems to reverse with the $sp2$ configuration providing a lower torque value as compared to the $sp1$ configuration for the TSR values of 6.35. On closer investigation with the thrust and power coefficient values obtained earlier for validation studies, a similar trend in terms of the power obtained by the configurations at varying TSR values is noticed.

3.7. Effects on circulation

The circulation distribution for the $sp1$, $sp2$ and clean case configurations are investigated to understand the effects of Gurney flaps on circulation. The circulation has been calculated by calculating the integral of the absolute velocities, see Equation (3). The
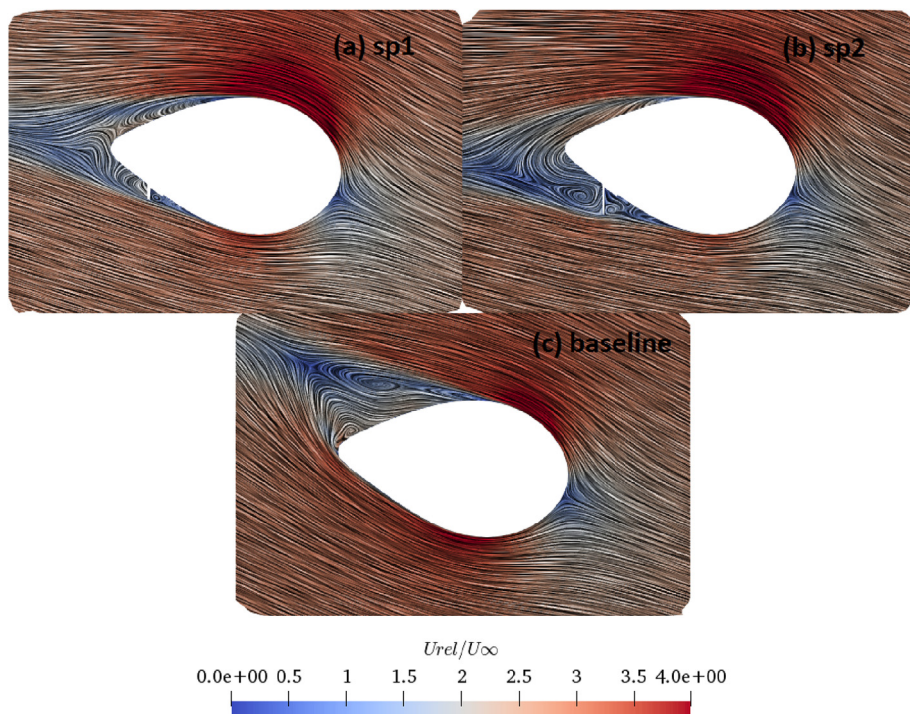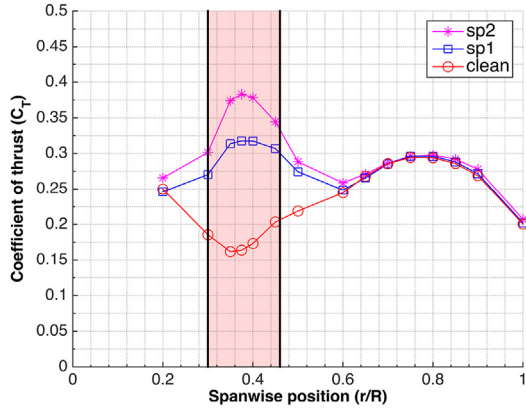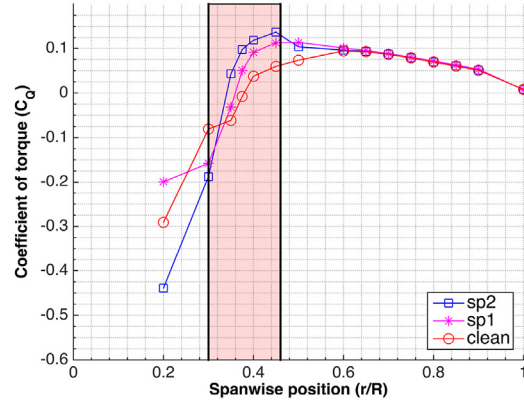

Fig. 14. Relative velocity flow field at $r/R = 0.4$ with $\lambda = 6.35$, (a) $sp1$ Gurney flap, (b) $sp2$ Gurney flap, (c) baseline rotor.

(a) C_T
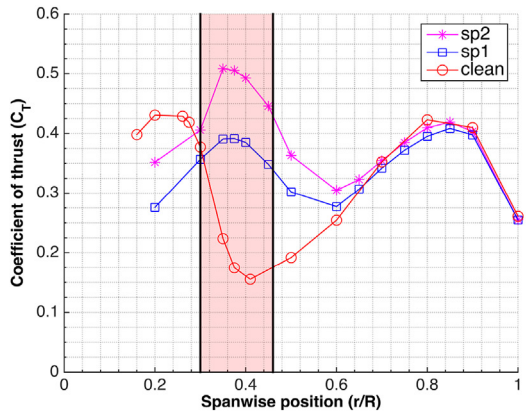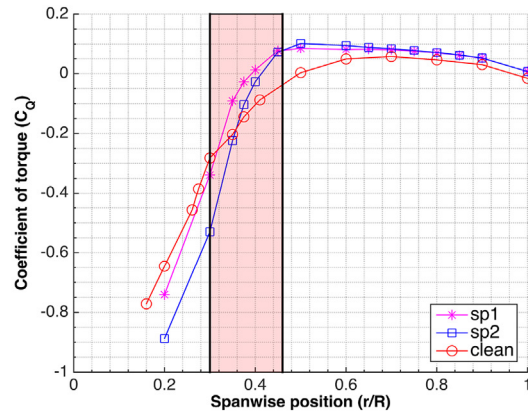
(b) C_Q

Fig. 15. C_T and C_Q distribution over blade span at $\lambda = 4.59$

(a) C_T

(b) C_Q

Fig. 16. C_T and C_Q distribution over blade span at $\lambda = 6.35$
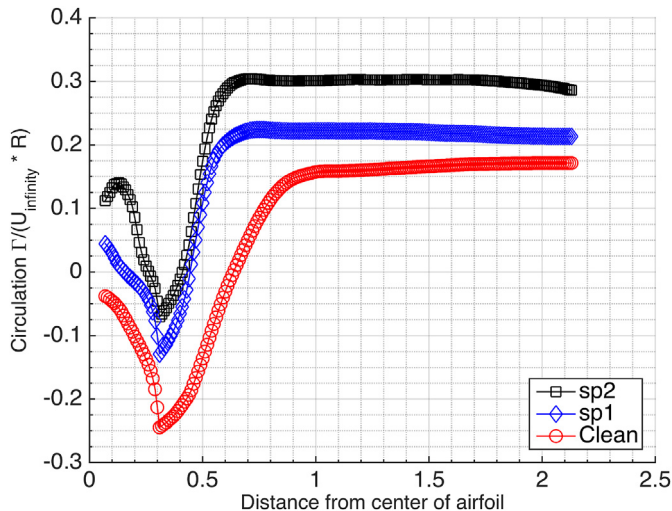

Fig. 17. Non-dimensionalized circulation convergence at $r/R = 0.35$ at $\lambda = 4.59$

closed loop was determined by varying lengths from the centre of the airfoil until a converged solution was obtained, see Fig. 17.

$$\Gamma = - \oint_C \overrightarrow{U} \cdot ds \tag{3}$$

Fig. 18 plots the non-dimensionalized circulation distribution at $\lambda = 4.59$ and $\lambda = 6.35$, respectively. Compared to the clean case, an increased circulation is seen at the Gurney flap regions in the $sp1$ and $sp2$ cases. Moreover, a higher circulation for the $sp2$ configuration at $\lambda = 4.59$ and a lower circulation at $\lambda = 6.35$ are observed when compared to the $sp1$ configuration. Since the lift of an airfoil is directly proportional to its circulation, and the power produced is mainly a direct consequence of the lift around the airfoil. The circulation obtained from the calculations is in accordance with the trend seen in the C_P values in Table 8 obtained for the cases at varying tip speed ratios.

4. Conclusions

This paper investigates the effects of root Gurney flaps on the aerodynamic performance of a horizontal axis wind turbine by
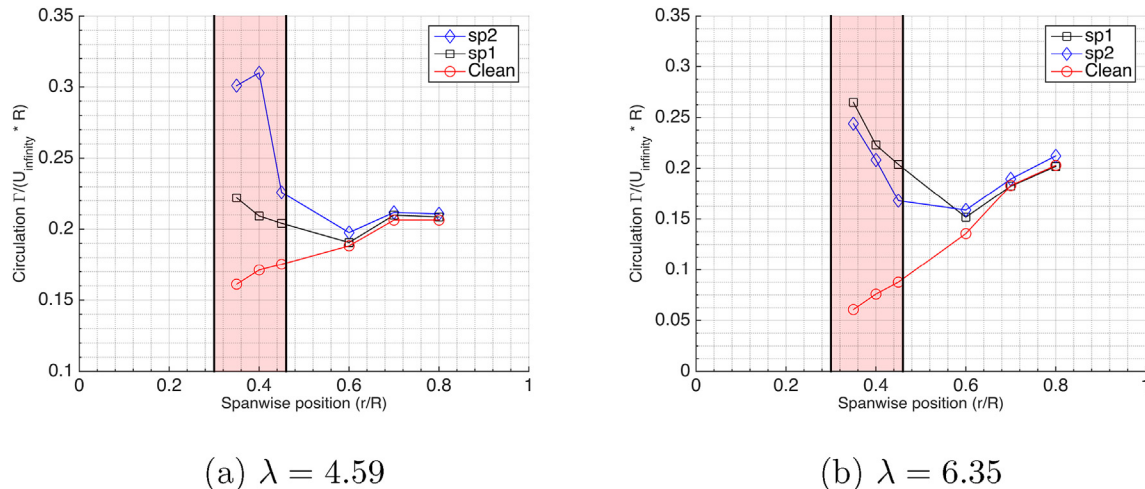
(a) $\lambda = 4.59$

(b) $\lambda = 6.35$

Fig. 18. Non-dimensionalized circulation distribution at $\lambda = 4.59$ and 6.35.

using computational fluid dynamics (CFD) method. Some observations and conclusions can be summarized as:

The root Gurney flaps tend to increase the local thrust and torque values over the blade. The thrust increases with the increase in Gurney flap height. Moreover, the root Gurney flap improves the power producing capabilities of wind turbines by a considerable amount for a specified tip speed ratio (21% increase at $\lambda = 6.35$). The $sp1$ Gurney flap is comparatively better in terms of power production than the $sp2$ Gurney flap. The reason being the full submergence of the $sp1$ Gurney in the boundary layer as compared to the $sp2$ configuration.

The pressure distribution indicates that the root Gurney flaps have a spanwise effect on the outboard part of the blade, which is further evidenced from the circulation distribution wherein a difference in circulation between the Gurney flap and baseline clean case is observed at the location $r/R = 0.6$. The separation analysis indicates that the separation location shifts towards the trailing edge with the presence of root Gurney flaps. The shift in separation location tends to increase with Gurney flap height and rotational velocity of the blade.

The open source CFD tool OpenFOAM provides a good prediction capability of the aerodynamic performance of a horizontal axis wind turbine with root Gurney flaps. A code-to-code comparison of CFD numerical results with BEMT method has a maximum relative difference of 6.67% in the thrust coefficient C_T for the mid-span of the wind turbine blade. Less than 10% relative difference is observed in the thrust and power coefficients for the baseline rotor and Gurney flap configurations between experimental measurement and CFD numerical results, except for the $sp2$ Gurney flap which has a higher relative difference of 14.1% at the higher tip speed ratio $\lambda = 6.35$.

References

[1] EWEA. Wind in power: 2015 european statistics. 2015. Available: http://www. ewea.org/fileadmin/files/library/publications/statistics/EWEA-Annual-Statistics-2015.pdf.

[2] Barlas Thanasis K, Van Kuik GAM. Review of state of the art in smart rotor control research for wind turbines. Prog Aerosp Sci 2010;46(1):1−27.

[3] Schepers JG, Boorsma K, Sørensen N, Sieros G, Rahimi H, Heisselmann H, Jost E, Lutz T, Maeder T, Gonzalez A, et al. Final results from the eu project avatar: aerodynamic modelling of 10 mw wind turbines. In: Journal of physics: conference series, vol. 1037. IOP Publishing; 2018. p. 022013.

[4] Gerard Schepers. Avatar: advanced aerodynamic tools of large rotors. In: 33rd wind energy symposium; 2015. p. 0497.

[5] Ferreira Carlos, Gonzalez A, Baldacchino Daniel, Aparicio M, Gómez S, Munduate X, Ramos García Néstor, Jens Nørkær Sørensen E Jost, Knecht S, et al. Results of the avatar project for the validation of 2d aerodynamic models with experimental data of the du95w180 airfoil with unsteady flap. In: Journal of physics: conference series, vol. 753. IOP Publishing; 2016. p. 022006.

[6] Baldacchino D, Manolesos M, Ferreira C, Gonzalez Salcedo A, Aparicio M, Chaviaropoulos T, Diakakis K, Florentie L, García NR, Papadakis G, et al. Experimental benchmark and code validation for airfoils equipped with passive vortex generators. In: Journal of physics: conference series, vol. 753. IOP Publishing; 2016. p. 022002.

[7] Liebeck Robert H. Design of subsonic airfoils for high lift. J Aircr 1978;15(9): 547−61.

[8] Anderson Jr John David. Fundamentals of aerodynamics. Tata McGraw-Hill Education; 2010.

[9] Cole Julia A, Vieira Bernardo AO, Coder James G, Premi Amandeep, Maughmer Mark D. Experimental investigation into the effect of gurney flaps on various airfoils. J Aircr 2013;50(4):1287−94.

[10] Roy Myose, Papadakis Michael, Heron Ismael. Gurney flap experiments on airfoils, wings, and reflection plane model. J Aircr 1998;35(2):206−11.

[11] Jang Cory S, Ross James C, Cummings Russell M. Numerical investigation of an airfoil with a gurney flap. Aircraft Des 1998;1(2):75−88.

[12] Henne Preston A, Robert III D Gregg. New airfoil design concept. J Aircr 1991;28(5):300−11.

[13] Kentfield JAC, Clavelle EJ. The flow physics of gurney flaps, devices for improving turbine blade performance. Wind Engineering; 1993. p. 24−34.

[14] Jain Shubham, Sitaram Nekkanti, Krishnaswamy Sriram. Effect of Reynolds number on aerodynamics of airfoil with gurney flap. Int J Rotating Mach 2015;2015.

[15] Giguere P, Lemay J, Dumas G. Gurney flap effects and scaling for low-speed airfoils. In: 13th applied aerodynamics conference; 1995. p. 1881.

[16] Patel Hardik S. A study on a cfd analysis of pressure difference on naca0012 airfoil by changing gurney flap height and angle of attack. IJAR - Indian J Appl Res 2015;5(4):838−43.

[17] Akay B, Ragni D, Ferreira CJ Simão, Bussel GJW. Experimental investigation of the root flow in a horizontal axis wind turbine. Wind Energy 2014;17(7): 1093−109.

[18] Herráez Iván, Akay Buşra, JW van Bussel Gerard, Peinke Joachim, Stoevesandt Bernhard. Detailed analysis of the blade root flow of a horizontal axis wind turbine. Wind Energy Sci 2016;1(2):89−100.

[19] Yu Guohua, Shen Xin, Zhu Xiaocheng, Du Zhaohui. An insight into the separate flow and stall delay for hawt. Renew Energy 2011;36(1):69−76.

[20] Sicot C, Devinant P, Loyer S, Hureau J. Rotational and turbulence effects on a wind turbine blade. investigation of the stall mechanisms. J Wind Eng Ind Aerodyn 2008;96(8−9):1320−31.

[21] Bangga Galih, Lutz Thorsten, Krämer Ewald. Root flow characteristics and 3d effects of an isolated wind turbine rotor. J Mech Sci Technol 2017;31(8): 3839−44.

[22] Kentfield JAC. Theoretically and experimentally obtained performances of gurney-flap equipped wind turbines. Wind Engineering; 1994. p. 63—74.

[23] Ebrahimi Abbas, Movahhedi Mohammadreza. Wind turbine power improvement utilizing passive flow control with microtab. Energy 2018;150:575—82.

[24] Zhu Haitian, Hao Wenxing, Chun Li, Ding Qinwei, Wu Baihui. A critical study on passive flow control techniques for straight-bladed vertical axis wind turbine. Energy 2018;165:12—25.

[25] Ismail Md Farhad, Krishna Vijayaraghavan. The effects of aerofoil profile modification on a vertical axis wind turbine performance. Energy 2015;80: 20—31.

[26] Menter Florian R. Improved two-equation k-omega turbulence models for aerodynamic flows. NASA STI/Recon Technical Report N, 93. 1992.

[27] Patankar SV, Spalding DB. A calculation procedure for heat, mass and momentum transfer in three-dimensional parabolic flows. Int J Heat Mass Transf 1972;15(10):1787—806.

[28] Greenshields Christopher J. Openfoam user guide. version, 3(1). OpenFOAM Foundation Ltd; 2015.

[29] Sørensen Niels N, Michelsen JA, Scott Schreck. Navier—Stokes predictions of the nrel phase vi rotor in the nasa ames 80 ft × 120 ft wind tunnel. Wind Energy: Int J Progress Appl Wind Power Conversion Technol 2002;5(2—3): 151—69.

[30] Farrell PE, Maddison JR. Conservative interpolation between volume meshes by local galerkin projection. Comput Methods Appl Mech Eng 2011;200(1—4): 89—100.